Title

Viscous control of cellular respiration by membrane lipid composition

Journal

Science, 362(6419)

ISSN

0036-8075

Authors

Budin, Itay

de Rond, Tristan

Chen, Yan

et al.

Publication Date

2018-12-07

DOI

10.1126/science.aat7925

Peer reviewed

Viscous control of cellular respiration by membrane lipid composition

Itay Budin[1,2]*, Tristan de Rond[1,3]†, Yan Chen[1,4], Leanne Jade G. Chan[1]‡, Christopher J. Petzold[1,4], Jay D. Keasling[1,2,5,6,7,8]*

Lipid composition determines the physical properties of biological membranes and can vary substantially between and within organisms. We describe a specific role for the viscosity of energy-transducing membranes in cellular respiration. Engineering of fatty acid biosynthesis in *Escherichia coli* allowed us to titrate inner membrane viscosity across a 10-fold range by controlling the abundance of unsaturated or branched lipids. These fluidizing lipids tightly controlled respiratory metabolism, an effect that can be explained with a quantitative model of the electron transport chain (ETC) that features diffusion-coupled reactions between enzymes and electron carriers (quinones). Lipid unsaturation also modulated mitochondrial respiration in engineered budding yeast strains. Thus, diffusion in the ETC may serve as an evolutionary constraint for lipid composition in respiratory membranes.

Cell membranes contain a multitude of distinct lipid components, but understanding how specific lipids influence biological func-tion is challenged by limited tools for their manipulation in vivo (*1*). Lipids can determine the physical characteristics of membranes (*2*), such as their viscosity, and these properties are homeostatically maintained by cells (*3*). In a classic example (fig. S1), the bacterium *Escherichia coli* increases the proportion of phospholipid acyl chains with double bonds (unsaturation) with decreasing growth temperatures, thereby maintaining a constant membrane viscosity (*4*). Similar lipid adaptations have been widely observed across organisms (*5*), suggesting that universal processes are mediated by membrane viscosity.

To investigate functions for membrane viscosity in vivo, we used metabolic engineering strategies to genetically modulate lipid composition in *E. coli* (fig. S2). FabB [β-ketoacyl-(acyl carrier protein) synthase I] carries out the rate-limiting step (*6*) for production of unsaturated fatty acids (UFAs) during fatty acid (FA) biosynthesis (Fig. 1A). We replaced the chromosomal copy of *fabB* with one under control of an L-arabinose–induced promoter (P_{BAD}) in a strain background that allows for titratable and homogeneous expression (*7*, *8*). After further tuning FabB levels with Shine-Dalgarno sequence variants (fig. S2C), we generated strains with controllable UFA amounts ranging from ~15% [the minimum amount for survival (*9*)] to ~80% of all FAs at 37°C (Fig. 1B). This modulation resulted primarily from the substitution of palmitate (C16:0) with vaccenate (C18:1) acyl chains (fig. S3A), which was observed in all phospholipid species (fig. S3B) and maintained throughout exponential growth (fig. S3D). Membrane ordering, as measured by steady-state anisotropy of diphenylhexatriene (DPH), steadily decreased with increasing lipid unsaturation in both inner membrane vesicles and protein-free liposomes (Fig. 1C). To estimate the effect of lipid unsaturation on membrane microviscosity, we measured diffusion coefficients of a nitrobenzoxadiazole (NBD)–conjugated phosphoethanolamine (PE) in giant *E. coli* inner membrane vesicles (GEVs) using fluorescence recovery after photobleaching (FRAP) (Fig. 1D). From these data, viscosities were derived by using the Saffman-Delbrück approximation (*10*) and showed a 10-fold range (~2 to 20 poise) as UFA content was modulated.

To identify physiological functions for UFAs, we correlated exponential growth rates with sampled lipid compositions in cells producing various amounts of FabB (Fig. 2A). Growth rates generally featured a biphasic dependence on lipid unsaturation: a sharp fitness cliff leading to a cessation of cell growth at low UFA levels (15 to 20% at 37°C, regime I), followed by increasing growth rates with higher UFA content (regime II). Regime I corresponded to the minimum amount of UFAs required (e.g., in fig. S1) and was observed under all conditions. By contrast, regime II was dependent on media with nonfermentable carbon sources, where growth is tightly coupled to adenosine 5′-triphosphate production through the electron transport chain (ETC) (*11*). Under fermentation conditions, when cells depend on glycolysis and are resistant to respiratory uncouplers (fig. S4D), growth rates were unaffected by UFAs in regime II (Fig. 2A). An analysis of stress response factors (Fig. 2B) showed that that low UFA levels caused both an oxidative stress response (OSR), which can result from ETC inhibition (*12*), and a heat shock response (HSR), which is activated by misfolded proteins (*13*). However, HSR activation occurred only as membranes approached a gel phase transition at the growth temperature (fig. S5B), and coincided with the mislocalization of membrane proteins (fig. S5C) and defects in cell division (fig. S5D). We therefore concluded that increasing proportions of saturated lipids trigger envelope stress as membranes become highly ordered (regime I), but also have a second, respiratory role over a broader range of stoichiometry (regime II).

When titrating FA synthesis, cellular respiration rates were tightly coupled to changes in unsaturated lipid content (Fig. 2C). This effect was independent of electron donor (for example, succinate or glycerol), electron acceptor (oxygen or nitrate), proton motive force (PMF) uncoupling, oxygen concentration (fig. S6A), and growth stage (fig. S6B). Wild-type cells overproducing UFAs through *fabB* overexpression or deletion of the regulator *fabR* similarly showed increased respiratory rates (fig. S6C). Under glucose fermentation, low lipid unsaturation led to the accumulation of pyruvate and lactate as secreted organic acids and a depletion of succinate. Such a mixed acid fermentation profile is consistent with ETC inhibition (fig. S6D).

To test if respiratory regulation occurs through a physical effect, we engineered a heterologous system for controlling membrane viscosity based on branched-chain fatty acid (BCFA) synthesis (Fig. 2D). Introduction of the *bkd* operon (for biosynthesis of β-ketoacids) and *fabH* (for initiation of BCFA synthesis) from *Bacillus subtilis* led to the accumulation of BCFAs in membrane lipids (fig. S7A), especially when amounts of UFA were low (fig. S7B). BCFA biosynthesis fluidized membranes (fig. S7C) and rescued growth defects from low lipid unsaturation (fig. S7D), even at amounts of UFAs that were otherwise lethal (fig. S7E). Uncoupled respiration rates were increased by BCFAs in addition to UFAs, and the effects of both FA species were preserved in isolated membrane vesicles (Fig. 2E).

We considered three mechanisms by which membrane viscosity could control ETC function. First, substrate uptake could be dependent on membrane properties, especially the passive permeation of oxygen. However, lipids act on respiration independently of substrate and oxygen concentrations (fig. S6A). Alternatively, viscosity could affect individual ETC enzymes, but their partial activities with soluble substrates were not inhibited by saturated lipids (fig. S6E). Lastly, we considered whether viscosity mediates collisions between electron carriers (ubiquinone) and enzyme complexes in the ETC, because a rate dependence on solvent viscosity is a hallmark of diffusion-limited reactions (*14*). On the basis of

[1]Joint BioEnergy Institute, 5885 Hollis Street, Emeryville, CA 94608, USA. [2]Department of Chemical and Biomolecular Engineering, University of California, Berkeley, Berkeley, CA 94720, USA. [3]Department of Chemistry, University of California, Berkeley, Berkeley, CA 94720, USA. [4]Biological Systems and Engineering, Lawrence Berkeley National Laboratory, Berkeley, CA 94720, USA. [5]Department of Bioengineering, University of California, Berkeley, Berkeley, CA 94720, USA. [6]QB3 Institute, University of California, Berkeley, Berkeley, CA 94270, USA. [7]The Novo Nordisk Foundation Center for Sustainability, Technical University of Denmark, Denmark. [8]Center for Synthetic Biochemistry, Institute for Synthetic Biology, Shenzhen Institutes for Advanced Technologies, Shenzhen, China.

***Corresponding author. Email: keasling@berkeley.edu (J.D.K.); budin@berkeley.edu (I.B.)** †Present address: Scripps Institution of Oceanography, University of California, San Diego, CA, USA. ‡Present address: Calico Life Sciences, South San Francisco, CA, USA.

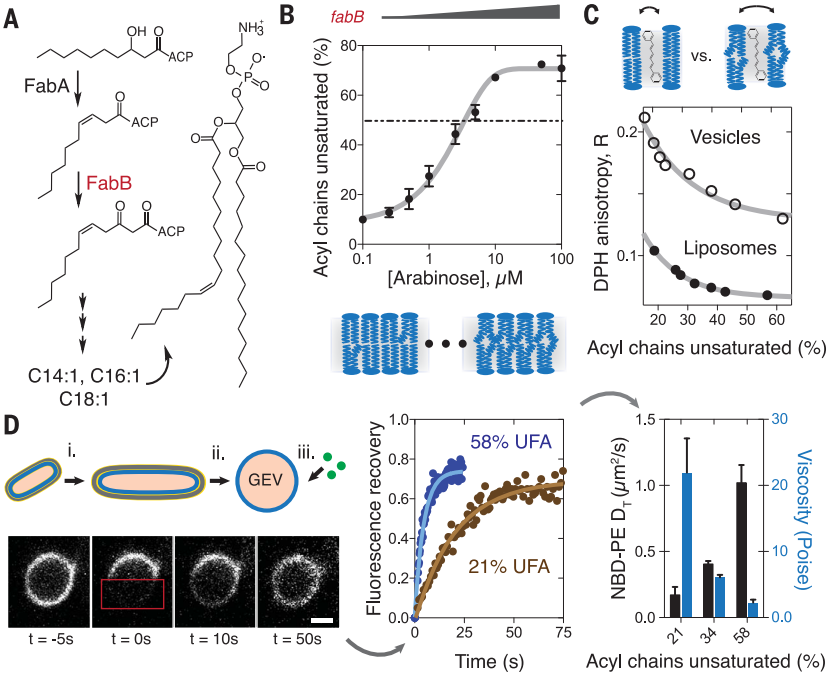

Fig. 1. Genetic titration of inner membrane viscosity in *E. coli*. (**A**) The pathway for bacterial UFA synthesis. The activity of FabB is rate-limiting for UFA synthesis and incorporation into phospholipids. (**B**) Titration of *fabB* expression with the P_{BAD} promoter modulates UFA stoichiometry as a function of inducer (arabinose) concentration. This leads to membranes with increasing amounts of *cis* double bonds, as shown in the model. Data are mean ± SD (N = 3 independent experiments). (**C**) Characterization of membrane ordering using DPH anisotropy. Higher anisotropy values indicate restricted motion of the probe and therefore a more ordered membrane. (**D**) A FRAP-based assay for measuring inner membrane diffusivities and its application in estimating membrane microviscosity. GEVs were generated by elongating cells with cephalexin (i). Cell walls were then digested (ii), thereby generating large, inner membrane vesicles to which lipid fluorophores can be added externally (iii). Shown is an experiment for a model substrate, NBD-PE, with recovery curves for two lipid compositions. Translational diffusion coefficients (D_T) were generated from the exponential constant of the recovery curve, and viscosity values were then estimated from these. Black bars show the calculated diffusion coefficients for NBD-PE (left y axis), and blue bars show the extrapolated estimated membrane viscosity (right y axis). Data are mean ± SEM (N = 5 independent experiments).

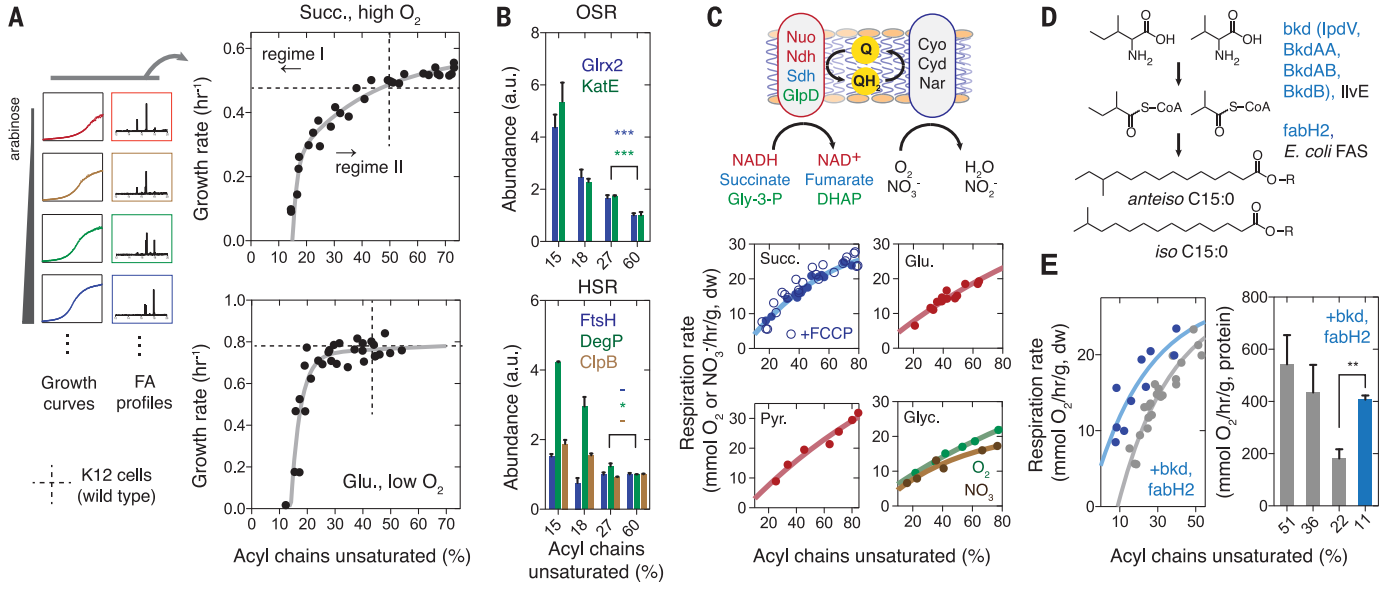

Fig. 2. Effects of FA composition on physiology and respiratory metabolism. (**A**) Growth rates and FA compositions were characterized for a series of batch cultures with various arabinose concentrations. The growth rate dependence on UFA levels occurs in two phases: a fitness cliff at low levels (regime I) and a gradual increase in growth rates at intermediate levels (regime II); these can be described by two exponential constants: k_1 ~ 0.6%$^{-1}$, k_2 ~ 0.03%$^{-1}$ at 37°C. The top plot shows the growth rate dependence under respiratory conditions and the bottom shows it for fermentative conditions, when regime II is absent. Succ., succinate; Glu., glucose. (**B**) Abundance of stress response factors in response to different proportions of unsaturated acyl chains. Data are mean ± SEM (N = 3), and overlaid are the results of t tests for significance between abundances in high (60%) and intermediate (27%) lipid unsaturation. ***p < 0.001, *p < 0.05; -, no significance. (**C**) The modular *E. coli* ETC consists of dehydrogenase (red) and terminal oxidase (blue) enzymes that react via an intermediate quinone pool. The different enzyme complexes used are color coded according to substrate. The corresponding respiration rates, as measured by oxygen or nitrate consumption, show a similar dependence (k ~ 0.01 to 0.03%$^{-1}$) on lipid unsaturation regardless of the electron donor or acceptor and whether the ETC is uncoupled by carbonyl cyanide-4-(trifluoromethoxy)phenylhydrazone (FCCP). Q, ubiquinone; NADH and NAD+, reduced and oxidized nicotinamide adenine dinucleotide; Gly-3-P, glycero-3-phosphate; DHAP, dihydroxyacetone phosphate; Pyr., pyruvate; Glyc., glycerol. (**D**) Heterologous biosynthesis of *anteiso* and *iso* BCFAs from amino acid precursors in *E. coli* using genes (highlighted in blue) from *B. subtilis*. (**E**) Effects of BCFA biosynthesis on uncoupled succinate respiration rates with various levels of lipid unsaturation (left). In purified membrane vesicles (right), the abundance of UFAs also mediates succinate respiration and a UFA deficiency can be rescued by BCFA biosynthesis, which increases respiration rates in UFA-depleted membranes (t test for significance, **p = 0.002). Data are mean ± SEM (N = 3 independent experiments).

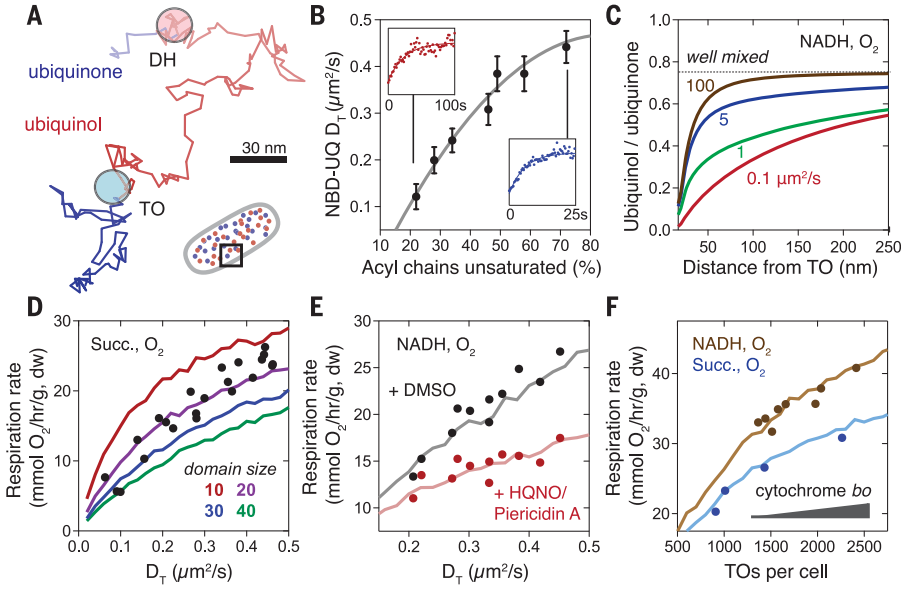

Fig. 3. Testing a diffusion-coupled reaction model for bacterial respiration. (**A**) A simulated random walk by a ubiquinone, which becomes reduced to ubiquinol (red) upon interaction with a DH domain and then reoxidized (blue) upon subsequent collisions with a TO, an oxygen-consuming reaction. The opacity of the path indicates progression during the time course (100 ms). (**B**) Experimental measurements of ubiquinone diffusivity in GEVs. Values are shown as averages from eight GEVs for each preparation. Solid line shows a quadratic function fit to the data and is used as a standard curve to convert lipid composition to diffusivity in subsequent experiments. Insets show example FRAP exponential recovery curves. Data are mean ± SEM (N = 5 independent experiments). (**C**) The distribution of the ubiquinone pool as a function of its diffusivity in whole-cell simulations, expressed as the steady-state average ubiquinol:ubiquinone ratio within a given radius of a TO. (**D**) Comparison of the simulated dependence of ubiquinone diffusivity (D_T) on respiration rates (solid lines) with measurements of uncoupled respiration in succinate medium (dots). Values in the legend are the domain size of the modeled ETC enzyme pair. (**E**) Modeling the effect of reducing enzymatic activity using the inhibitors *N*-oxo-2-heptyl-4-hydroxyquinoline (HQNO) and piericidin A, which act on TOs and NADH DH, respectively. Simulated rates of NADH-linked respiration (solid lines), modeled using 20-mer homotypic domains, are shown alongside uncoupled respiration rates in pyruvate medium (dots) under various UFA levels with HQNO (20 μM) and piericidin A (100 nM), or with no inhibitors (DMSO, dimethyl sulfoxide). (**F**) The effect of changes in TO concentration—achieved by titrating expression of *cyoABCD*—on respiratory rates. Simulation results (solid lines) are superimposed with experimental measurements of NADH respiration with pyruvate (brown) and succinate respiration (blue); measured TO abundance includes both aerobic cytochrome oxidases (*bo* and *bd*-I).

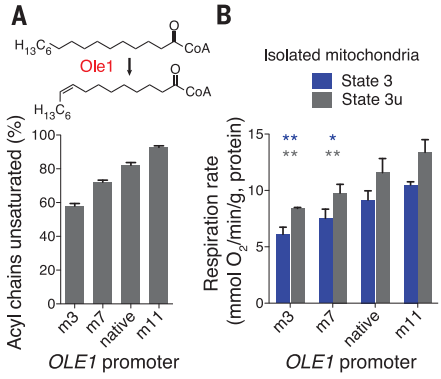

Fig. 4. Lipid-mediated respiration in mitochondria. (**A**) The desaturase Ole1 generates all UFAs in yeast. Unsaturated lipid composition is controlled by the promoter driving expression of *OLE1*—either the native one, or one of three variants (m3, m7, m11) in engineered strains. (**B**) Mitochondrial respiration rates in coupled (state 3, 0.5 mM ADP) and uncoupled (state 3u, 4 μM FCCP) conditions corresponded with unsaturated lipid content. Mitochondria were incubated with 5 mM succinate as a substrate. Data are mean ± SEM (N = 3 independent experiments), and overlaid are the results of t tests for significance against m11. $^{**}p < 0.01$, $^{*}p < 0.05$.

the pool behavior of quinones (*15*, *16*), their diffusion between complexes has been proposed to be rate-limiting in mitochondrial respiration (*17*, *18*), but this concept was disputed (*19*, *20*).

To investigate the role of diffusion in cellular respiration, we developed a model of the *E. coli* ETC based on the Brownian motion of membrane components and their collision-mediated reactions (Fig. 3A and fig. S8). As inputs, we combined activities of purified ETC enzymes—dehydrogenases (DHs) and terminal oxidases (TOs)—with measurements of their absolute abundances using quantitative mass spectrometry (supplementary materials) and their organization into homotypic domains as previously described (*21*, *22*). Whole-cell simulations were then carried out to quantify the rate of electron transfer as a function of ubiquinone diffusivity. To measure this parameter, we used FRAP experiments with an NBD-conjugated ubiquinone (NBD-UQ, fig. S9), thereby defining lipid-dependent diffusion coefficients (Fig. 3B).

Our model predicted that ubiquinone diffusivity controls respiratory flux in membranes spanning the tested range of lipid compositions. Diffusion control was measured by quinone anisotropy, with reduced electron carriers becoming depleted in the vicinity of TOs (Fig. 3C and movie S1). As diffusion increased, the quinone pool became well-mixed and rates were increasingly determined by enzyme activities (fig. S8B). Simulations matched measured respiratory rates when enzymes were modeled as domains of 10 to 30 proteins (Fig. 3D), consistent with their reported organization in cells (*21*). Simulations also predicted changes to respiratory rates upon inhibition of ETC enzymes (Fig. 3E), which reduces the rate dependence on diffusion, and during genetic titration of TO abundance (Fig. 3F), which modulates the average diffusion distance for a reactive collision.

As in bacteria, respiration in eukaryotic mitochondria is also dependent on quinone-mediated electron transfer. In animal models, correlations between mitochondrial FA composition and metabolic rate have been observed between species (*23*), and membrane-fluidizing steroids have been shown to promote respiration (*24*). To test whether lipid composition controls mitochondrial respiration, we used a set of constitutive promoters to manipulate Ole1 (acyl–coenzyme A desaturase) levels in *Saccharomyces cerevisiae* (Fig. 4A). In strains that showed regular mitochondrial morphology (fig. S10A), greater lipid unsaturation led to increased respiratory activity but, as in *E. coli*, did not inhibit fermentative metabolism or growth (fig. S10, B and C). In isolated mitochondria, UFA content controlled the rate of respiration coupled to adenosine 5′-diphosphate (ADP) phosphorylation (state 3) and uncoupled (state 3u) from the PMF (Fig. 4B).

The role for diffusion in respiration provides a functional rationale for variations in lipids within and between cells. In eukaryotes, lipid species that increase membrane viscosity—sterols and sphingolipids—are depleted from energy-transducing membranes (*25*). In prokaryotes, analogous rigidifying lipids, such as hopanoids and archaeal ether lipids, are associated with niches where the robustness of the membrane as a permeability barrier is paramount over rapid metabolic activity (*26*). Such a trade-off is evident in *E. coli*, which eliminates lipid unsaturation through cyclopropanation during stationary phase to survive in acidic conditions (*27*). Localizing ETCs to fluid internal membranes while maintaining rigid outer membranes could thus have served as an advantage during the evolution of dedicated metabolic organelles. In some mitochondria, ETCs are additionally organized into supercomplexes of respiratory enzymes (*28*, *29*).

In our simulations, tethering of DH and TO enzymes increased respiration rates and reduced anisotropy in the quinone pool (fig. S11, movie S2, supplementary text). A diffusion-coupled reaction model could therefore be important for understanding how the interplay between lipid composition, enzymatic activity, and membrane organization dictates respiratory function in a wide range of systems.

REFERENCES AND NOTES

1. E. Muro, G. E. Atilla-Gokcumen, U. S. Eggert, *Mol. Biol. Cell* **25**, 1819–1823 (2014).
2. T. Harayama, H. Riezman, *Nat. Rev. Mol. Cell Biol.* **19**, 281–296 (2018).
3. R. Covino *et al*., *Mol. Cell* **63**, 49–59 (2016).
4. M. Sinensky, *Proc. Natl. Acad. Sci. U.S.A.* **71**, 522–525 (1974).
5. J. R. Hazel, *Annu. Rev. Physiol.* **57**, 19–42 (1995).
6. Y. Feng, J. E. Cronan, *J. Biol. Chem.* **284**, 29526–29535 (2009).
7. A. Khlebnikov, K. A. Datsenko, T. Skaug, B. L. Wanner, J. D. Keasling, *Microbiology* **147**, 3241–3247 (2001).
8. M. A. Kay, C. Y. He, Z. Y. Chen, *Nat. Biotechnol.* **28**, 1287–1289 (2010).
9. J. E. Cronan Jr., E. P. Gelmann, *J. Biol. Chem.* **248**, 1188–1195 (1973).
10. P. G. Saffman, M. Delbrück, *Proc. Natl. Acad. Sci. U.S.A.* **72**, 3111–3113 (1975).
11. K. B. Andersen, K. von Meyenburg, *J. Bacteriol.* **144**, 114–123 (1980).
12. A. N. Woodmansee, J. A. Imlay, *J. Biol. Chem.* **277**, 34055–34066 (2002).
13. T. Yura, K. Nakahigashi, *Curr. Opin. Microbiol.* **2**, 153–158 (1999).
14. A. C. Brouwer, J. F. Kirsch, *Biochemistry* **21**, 1302–1307 (1982).
15. A. Kröger, M. Klingenberg, *Eur. J. Biochem.* **34**, 358–368 (1973).
16. P. R. Rich, *FEBS Lett.* **130**, 173–178 (1981).
17. B. Chazotte, C. R. Hackenbrock, *J. Biol. Chem.* **264**, 4978–4985 (1989).
18. S. Gupte *et al*., *Proc. Natl. Acad. Sci. U.S.A.* **81**, 2606–2610 (1984).
19. C. Bianchi, M. L. Genova, G. Parenti Castelli, G. Lenaz, *J. Biol. Chem.* **279**, 36562–36569 (2004).
20. R. Fato, M. Battino, M. Degli Esposti, G. Parenti Castelli, G. Lenaz, *Biochemistry* **25**, 3378–3390 (1986).
21. I. Llorente-Garcia *et al*., *Biochim. Biophys. Acta* **1837**, 811–824 (2014).
22. T. Lenn, M. C. Leake, C. W. Mullineaux, *Mol. Microbiol.* **70**, 1397–1407 (2008).
23. M. D. Brand, P. Couture, P. L. Else, K. W. Withers, A. J. Hulbert, *Biochem. J.* **275**, 81–86 (1991).
24. M. J. Torres *et al*., *Cell Metab.* **27**, 167–179.e7 (2018).
25. G. van Meer, D. R. Voelker, G. W. Feigenson, *Nat. Rev. Mol. Cell Biol.* **9**, 112–124 (2008).
26. D. L. Valentine, *Nat. Rev. Microbiol.* **5**, 316–323 (2007).
27. Y.-Y. Chang, J. E. Cronan Jr., *Mol. Microbiol.* **33**, 249–259 (1999).
28. D. Milenkovic, J. N. Blaza, N. G. Larsson, J. Hirst, *Cell Metab.* **25**, 765–776 (2017).
29. J. A. Letts, K. Fiedorczuk, L. A. Sazanov, *Nature* **537**, 644–648 (2016).

ACKNOWLEDGMENTS

N. Oppenheimer, H. Stone, and D. Arlow contributed helpful discussions, and the Coates (University of California, Berkley) and Lippincott-Schwartz (Janelia Research Campus) labs contributed experimental assistance. **Funding:** This work was part of the DOE Joint BioEnergy Institute supported by the U.S. Department of Energy, Office of Science, Office of Biological and Environmental Research, through contract DE-AC02-05CH11231 between Lawrence Berkeley National Laboratory and the U.S. Department of Energy. This work was also supported by National Science Foundation grants MCB-1442724 and MCB-1715681 to J.D.K, and a Junior Fellowship to I.B. from the Miller Institute for Basic Research. **Author contributions:** I.B. designed the study and performed the experiments. T.d.R. developed the model with I.B. and performed chemical synthesis. Y.C., L.J.G.C., and C.J.P. performed protein mass spectrometry analysis. All authors wrote the paper and discussed the results. **Competing interests:** J.D.K. has a financial interest in Amyris, Lygos, Demetrix, Constructive Biology, Maple Bio, and Napigen. The research described in this publication is not related to the work of these companies. **Data and material availability:** All strains are available from the Joint BioEnergy Institute public registry (https://public-registry.jbei.org). Protein mass spectrometry SRM data and methods are available at Panamoramaweb (http://goo.gl/JJySak). The ETC simulation script, written in Python, as well as examples of commands to invoke it, are available at GitHub (http://github.com/tderond/Budin2018).